JOURNAL OF GEOPHYSICAL RESEARCH, VOL. 101, NO. C1, PAGES 1295–1308, JANUARY 15, 1996

Cool-skin and warm-layer effects on sea surface temperature

C. W. Fairall,[1] E. F. Bradley,[2] J. S. Godfrey,[3] G. A. Wick,[4] J. B. Edson,[5] and G. S. Young[6]

Abstract. To obtain bulk surface flux estimates approaching the ±10 W m^{-2} accuracy desired for the Tropical Ocean-Global Atmosphere Coupled Ocean-Atmosphere Response Experiment (COARE) program, bulk water temperature data from ships and buoys must be corrected for cool-skin and diurnal warm-layer effects. In this paper we describe two simple scaling models to estimate these corrections. The cool-skin model is based on the standard *Saunders* [1967] treatment, including the effects of solar radiation absorption, modified to include both shear-driven and convectively driven turbulence through their relative contributions to the near-surface turbulent kinetic energy dissipation rate. Shear and convective effects are comparable at a wind speed of about 2.5 m s^{-1}. For the R/V *Moana Wave* COARE data collected in the tropical western Pacific, the model gives an average cool skin of 0.30 K at night and an average local noon value of 0.18 K. The warm-layer model is based on a single-layer scaling version of a model by *Price et al.* [1986]. In this model, once solar heating of the ocean exceeds the combined cooling by turbulent scalar heat transfer and net longwave radiation, then the main body of the mixed layer is cut off from its source of turbulence. Thereafter, surface inputs of heat and momentum are confined to a depth D_T that is determined by the subsequent integrals of the heat and momentum. The model assumes linear profiles of temperature-induced and surface-stress-induced current in this "warm layer." The model is shown to describe the peak afternoon warming and diurnal cycle of the warming quite accurately, on average, with a choice of a critical Richardson number of 0.65. For a clear day with a 10-m wind speed of 1 m s^{-1}, the peak afternoon warming is about 3.8 K with a warm-layer depth of 0.7 m, decreasing to about 0.2 K and 19 m at a wind speed of 7 m s^{-1}. For an average over 70 days sampled during COARE, the cool skin increases the average atmospheric heat input to the ocean by about 11 W m^{-2}; the warm layer decreases it by about 4 W m^{-2} (but the effect can be 50 W m^{-2} at midday).

1. Introduction

Sea surface temperature (SST) is a key variable driving air-sea interaction. SST and air-sea fluxes were a dominant component of the study of the tropical western Pacific warm pool in the Tropical Ocean-Global Atmosphere (TOGA) Coupled Ocean-Atmosphere Response Experiment (COARE) held in 1992–1993 [*Webster and Lukas*, 1992]. Uncertainties in air-sea temperature difference represent a major uncertainty in assessing the heat balance of the warm pool [*Lukas*, 1989]. *Fairall et al.* [1996a] have shown that to estimate this heat balance to an accuracy of 10 W m^{-2} requires specification of the SST to an accuracy of ±0.2 K.

Bulk flux routines are based on the empirical relationship between the turbulent fluxes and the air-sea contrasts of wind, humidity, and temperature; the SST is the lower thermal boundary condition. Logically, the proper temperature is taken at the air-sea interface T_s; this is essentially the temperature sensed by an infrared radiometer. However, the measurement of T_s by infrared radiometer requires careful correction for reflected atmospheric radiance and places extreme demands on the absolute calibration accuracy and stability of the device. Inexpensive, accurate, and reliable instruments that can routinely do this job are not available, so we must use in situ sensors placed in the water. These so-called bulk temperature sensors may use ship intakes at 2–10 m depth or floating thermistors at a few centimeters depth. To obtain the correct interfacial temperature, these bulk temperatures must be corrected for the warm layer and the cool skin:

$$T_s = T_m(z_r) - \Delta T_c + \Delta T_w(z_r) \quad (1)$$

where $T_m(z_r)$ is determined from our subsurface in situ temperature measurements (at reference depth z_r), ΔT_c is the cool-skin correction, and $\Delta T_w(z_r)$ is the warm-layer correc-

[1]Environmental Technology Laboratory, NOAA, Boulder, Colorado.
[2]Centre for Environmental Mechanics, Commonwealth Scientific and Industrial Research Organization, Canberra, Australian Capital Territory, Australia.
[3]Division of Oceanography, Commonwealth Scientific and Industrial Research Organization, Hobart, Tasmania, Australia.
[4]Colorado Center for Astrodynamics Research, University of Colorado, Boulder.
[5]Applied Ocean Physics and Engineering Department, Woods Hole Oceanographic Institution, Woods Hole, Massachusetts.
[6]Department of Meteorology, Pennsylvania State University, University Park.

Paper number 95JC03190.
0148-0227/96/95JC-03190$05.00

tion. Whereas the cool skin is unambiguously above any realistic in situ sensor we are likely to use, this is not true for the warm layer. Thus the warm-layer correction depends on the depth of our sensor; the shallower the sensor, the smaller the correction. The warm layer is a region in the upper few meters of the ocean where solar radiation has caused significant warming relative to the deeper mixed-layer temperature. Warm layers occur during the day when temperature stratification caused by absorption of the solar flux is sufficiently strong to suppress shear-induced mixing and can be of the order of 3 K. Thus the warm layer is a diurnal phenomenon, but for economy of expression we shall refer to it as the warm layer rather than the diurnal warm layer. The cool skin is a layer in the upper few millimeters of the ocean caused by the combined cooling effects of the net longwave radiation R_{nl}, the sensible heat flux H_s, and the latent heat flux H_l. The cool skin is of the order of 0.1–0.5 K and is almost always present, although its total effect may be compensated by the presence of a warm layer.

Incorrect specification of the surface boundary condition leads to direct errors in the net longwave radiative flux and bulk-derived values for latent and sensible heat flux; an indirect error in bulk stress values occurs through specification of the stability. By comparing fluxes computed with bulk and IR SSTs, *Coppin* [1994] showed that the error in the total surface heat budget can exceed 100 W m^{-2}. In the interest of improving the accuracy of bulk flux computations, we have investigated various methods for correcting bulk temperature measurements for the cool skin and the warm layer. In section 2 we examine the physical principles, experimental basis, and the implementation of the cool-skin correction, including the development of a wind-speed-dependent form of the Saunders coefficient that accounts for the effects of buoyancy-generated turbulence at low wind speeds. In section 3 we discuss the warm layer and show how it is described by the Price-Weller-Pinkel (PWP) surface layer model [*Price et al.*, 1986]. The PWP scaling model uses a critical Richardson number criterion applied to the momentum and heat accumulated in the near surface of the ocean to determine the depth of the stably stratified turbulent warm layer. The integration of these models into a bulk flux algorithm is described in section 4. Both the cool-skin and warm-layer models are tested against data obtained in TOGA COARE. Air-sea flux and in situ water temperature measurements taken aboard the R/V *Moana Wave* make up the bulk of this analysis, but high-quality IR radiometer measurements of sea surface interfacial temperature made aboard the R/V *Vickers* and the R/V *Franklin* are also used. Our conclusions are given in section 5.

2. The Cool Skin

2.1. Cool-Skin Background

The basic physics of the cool skin was described by *Saunders* [1967]. The total cooling at the interface Q is given by

$$-Q = R_{nl} - H_s - H_l \tag{2}$$

where we use the normal meteorological sign conventions (e.g., $R_{nl} = R_{\downarrow l} - R_{\uparrow l}$), and a positive value for Q represents cooling of the water. Because this cooling is realized at the interface (the longwave penetration depth is about 10 μm), the temperature gradient at the interface is defined by molecular thermal conductive processes:

$$k \frac{\partial T}{\partial z}\Big|_0 = Q \tag{3}$$

where k is the thermal conductivity of water, z is the vertical ordinate (zero at the surface and positive downward), and T is the temperature profile. Away from the interface the temperature gradient is quickly destroyed by turbulent mixing. Thus the cool-skin temperature change is confined to a region of thickness δ, which is referred to as the molecular sublayer. From (3), we can see that

$$\Delta T_c \sim Q\delta/k \tag{4}$$

where we use the convention that ΔT_c is positive if the surface is cooler than the bulk. We can estimate δ by assuming that it is proportional to the Kolmogorov microscale [*Panofsky and Dutton*, 1984]

$$\delta \sim (\nu^3/\varepsilon)^{1/4} \tag{5}$$

where ν is the kinematic viscosity and ε is the rate of dissipation of turbulent kinetic energy. For turbulence generated by surface shear, ε scales as u_{*w}^3/z, where u_{*w} is the friction velocity (in the water); for turbulence generated by convection, ε scales as $\alpha g Q_b/(\rho c_p)$, where α is the thermal expansion coefficient, Q_b is the virtual surface cooling that includes the buoyancy effects of salinity due to evaporation, g is the acceleration of gravity, ρ is the density, and c_p is the specific heat of water.

For the shear-generated turbulence regime we set $\delta = z$ to determine the dissipation rate in the diffusion sublayer (the subscript s denotes specifications of δ and ΔT_c for the shear-driven regime),

$$\delta_s = \frac{\lambda\nu}{u_{*w}}$$
$$\Delta T_{cs} = \frac{\lambda Q\nu}{k u_{*w}} \tag{6}$$

where λ is an empirical coefficient determined by simultaneous measurements of ΔT_c, Q, and u_{*w}. For convectively generated turbulence, (5) leads to a minus one-fourth power dependence of δ on Q_b; the form that is usually used follows from Rayleigh number scaling of free convection and is

$$\delta_b = \left(\frac{k^2\nu}{A^3 g\alpha\rho c_p Q_b}\right)^{1/4}$$
$$\Delta T_{cb} = \left(\frac{\nu}{A^3 g\alpha\rho c_p k^2}\right)^{1/4} Q/Q_b^{1/4} \tag{7}$$

where A is an empirical constant and the subscript b denotes the buoyancy-driven regime. The form of the virtual cooling follows from the relation of the density flux to the thermal and salinity fluxes [*Paulson and Simpson*, 1981]

$$Q_b = Q + \left(\frac{S\beta c_p}{\alpha L_e}\right) H_l \tag{8}$$

where S is the mean salinity, β is the salinity expansion coefficient, and L_e is the latent heat of vaporization. Note that $S\beta$ is relatively constant in the ocean ($\approx$0.026), but α decreases from about 3×10^{-4} K^{-1} in the tropics to near zero in polar regions. Thus in the COARE region the parenthetical factor in the second term of (8) has a value of about 0.14, and in the light wind conditions where (7) is applicable, Q_b will differ from Q by no more than 10%.

2.2. The Saunders Constants

Numerous studies of λ have been performed over the ocean (see *Robinson et al.* [1984] or *Fedorov and Ginsburg* [1992] for reviews). Fedorov and Ginsburg listed 12 different field studies of λ, a typical value being 6. There are reports of λ increasing with wind speed, and there are reports of λ decreasing with wind speed. Because many of the studies ignore the buoyancy-driven regime, their smaller values of λ in light winds are quite consistent with (7). Most of the studies suffer from either crude determinations of at least one of the key terms in computing Q or inadequate accuracy for T_s. Consider that a typical value for ΔT_c is about 0.3 K, but an accuracy better than $\pm$0.1 K for T_s has yet to be demonstrated. Even with careful longwave radiative flux measurements, uncertainties in bulk flux computations (particularly in the earlier studies) suggest that Q is uncertain by at least 10%. Thus 30% systematic errors in estimates of λ are difficult to avoid.

For example, *Hasse* [1971] used empirical formulas to estimate Q and determined T_s by equating it to the measured air temperature when the gradient was small. *Paulson and Simpson* [1981] used bulk formulas for the turbulent fluxes and direct measurements of R_{nl}, but T_s was determined from a narrowband IR thermometer corrected for sky reflection with broadband, global IR flux data. Furthermore, the absolute calibration of the IR thermometer was adjusted with a polynomial of the order of 5 generated by minimizing the rms difference between the measured values of ΔT_c and the *Saunders* [1967] formula. Two recent experiments [*Schluessel et al.*, 1990; *Coppin et al.*, 1991] have featured improved IR thermometers and flux measurements, although their daytime results are confused by the effects of the warm layer. Typical nighttime values of ΔT_c are about 0.3 K and are consistent with λ between 4 and 8; they also confirm that a constant λ (or even a simple linear regression approach) is not satisfactory.

Fedorov and Ginsburg [1992] listed three laboratory and one field study of the convective coefficient A; values vary from 0.16 to 0.26. We are going to use 0.23 (i.e., $A^{-3/4} = \lambda/2 = 3.0$), which is midway between the value 0.2 suggested by *Saunders* [1967] and the value 0.25 recommended by Fedorov and Ginsburg (from *Shigayeva et al.*'s [1982] field program in the Sea of Japan). Combined with $\lambda = 6$, this will lead to a shear-driven to convective-driven transition beginning at about 4 m s^{-1} for typical values of Q; this is consistent with *Paulson and Simpson*'s [1981, Figure 8] results.

2.3. Combining Convective and Shear Relationships

The convective and shear forms for δ can be smoothly blended by approximating their relative contributions to the dissipation rate. For example, the Kansas experiment [*Wyngaard and Cote*, 1971] yields

$$\varepsilon \propto \left(\frac{u_*^3}{z}\right)\left(1 + |z/L|^{2/3}\right)^{3/2} \tag{9}$$

where L is the Monin-Obukhov stability length. In the limit that $|z/L| \to 0$ (i.e., neutral conditions), ε will approach u_*^3/z, which, for $z = \delta$ and combined with (5), will yield (6) within a constant. Similarly, when $|z/L|$ becomes large, ε will approach $g\alpha Q_b/(\rho c_p)$, which, when combined with (5), will yield (7) within a constant. We can approximate (9) as

$$\varepsilon \approx \frac{u_{*w}^3}{\delta\lambda^3} + \frac{A^3 g\alpha\rho c_p Q_b \nu^2}{k^2} \tag{10}$$

where the shear term has been written to yield (6) directly in the neutral limit and the buoyant term to be consistent with (7). Dividing by $(\nu)^3$ yields

$$\frac{1}{\delta^3} = \frac{1}{\delta_s^3} + \frac{1}{\delta_b^3}\frac{\delta}{\delta_b} \tag{11}$$

We assume that the δ/δ_c term on the right-hand side of (11) is about 1, and we use (11) to incorporate these effects into a λ coefficient that is not constant but depends on conditions. Thus

$$\delta = \frac{\lambda\nu}{(\rho_a/\rho)^{1/2} u_{*a}} \tag{12}$$

where ρ_a is the density of air and u_{*a} is the atmospheric friction velocity (we have assumed that the stress is the same on the atmospheric and oceanic sides of the interface and expressed the result in terms of the atmospheric variables, which are more easily determined). The cool skin is given by

$$\Delta T_c = \frac{Q\delta}{k} \tag{13}$$

$$\lambda = 6\left[1 + \left(\frac{Q_b 2^4 g\alpha\rho c_p \nu^3}{u_{*a}^4 (\rho_a/\rho)^2 k^2}\right)^{3/4}\right]^{-1/3} \tag{14}$$

Shear and convective effects are comparable when the term inside the three-quarter power is of the order of 1 (yielding a value for λ of 4.8). This occurs (using parameters appropriate for COARE) when

$$u_{*a}^4 = 4.4 \times 10^{-7} Q_b \tag{15}$$

which implies $u_{*a} \approx 0.08$ m s^{-1} and $u \approx 2.5$ m s^{-1}.

2.4. Solar Radiation Absorption Profile

The final point we must consider is the effect of solar heating. *Saunders* [1967] estimated that about 5% of the net

solar flux will be absorbed in the nearest 1 mm of the water surface and that this heat acts to reduce the cooling effects of Q. If we define δS_c as the mean value of solar flux absorbed within the cool-skin sublayer, then we simply replace Q in (13) with $Q - S_c$. Following *Saunders* [1967] and *Paulson and Simpson* [1981], we represent $\delta S_c = f_c S_{ns}$, where

$$f_c = f(\delta) = \sum_{i=1}^{N} F_i \left\{1 - \frac{\gamma_i}{\delta}\left[1 - \exp(-\delta/\gamma_i)\right]\right\} \quad (16)$$

which describes the absorption in nine wavelength bands of amplitude F_i and absorption length γ_i (see Table 1). The first four bands have absorption scales much greater than 1 mm, and the last four have absorption scales much less than 1 mm. Thus we can approximate the mean absorption in the sublayer ($\delta < 1$ cm) as

$$f_c = \left\langle\left\{0.137 + 11\delta - \frac{6.6 \times 10^{-5}}{\delta}\left[1 - \exp(-\delta/8 \times 10^{-4})\right]\right\}\right\rangle \quad (17)$$

where 0.137 is the sum of the last five F_i, and 11 is one half the sum of the first four values of F_i/γ_i. For $\delta = 1$ mm, δS_c is 0.091 R_{ns}; consequently, even for quite thin sublayers, at least 5% of net solar will be absorbed.

It is not clear that such a complicated scheme for adjusting this correction depending on the actual value of δ is justified by the present accuracy of λ and the specification of (16) or its simplified form, (17). *Paulson and Simpson* [1981] obtained better results with (16) compared to the simple approximation $\delta S_c = 0.19\, R_{ns}$ suggested by *Hasse* [1971], but a reduction of the coefficient from 0.19 to 0.10 would give reasonable agreement. However, for the very light winds often encountered in COARE we will probably need to use (17) because δ will tend to be large. These results imply that for wind speeds below about 1 m s^{-1} the solar flux absorbed within δ will exceed the total cooling at the interface described by (2). Under these conditions there may be no net cool skin near noon (indeed, there may even be a warm skin), irrespective of any additional warm-layer effects. On those occasions when $Q - \delta S_c$ is negative, then there is no cool skin and ΔT_c is set to zero (presently, no warm skin as permitted by the model).

Table 1. Exponential Coefficient for Nine-Wavelength Fit to Absorption of Solar Radiation in Seawater

i	Wavelength, μm	F_i	γ_i, m	F_i/γ_i
1	0.2–0.6	0.237	34.8	6.8×10^{-3}
2	0.6–0.9	0.360	2.27	1.6×10^{-1}
3	0.9–1.2	0.179	3.15×10^{-2}	5.7
4	1.2–1.5	0.087	5.48×10^{-3}	1.6×10^{1}
5	1.5–1.8	0.080	8.32×10^{-4}	9.7×10^{1}
6	1.8–2.1	0.0246	1.26×10^{-4}	1.9×10^{2}
7	2.1–2.4	0.025	3.13×10^{-4}	8.0×10^{1}
8	2.4–2.7	0.007	7.82×10^{-5}	9.0×10^{1}
9	2.7–3.0	0.0004	1.44×10^{-5}	2.8×10^{1}

Data are based on *Paulson and Simpson* [1981]. Variables are defined as follows: i, wavelength number; F_i, amplitude; and γ_i, absorption length.

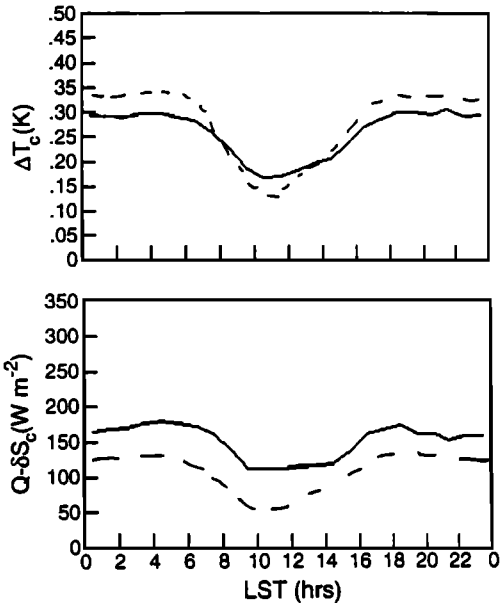

Figure 1. Average diurnal behavior from R/V *Moana Wave* Coupled Ocean-Atmosphere Response Experiment (COARE) data computed with the cool-skin model, all data (solid lines) and wind speed less than 4.0 m s^{-1} (dashed lines); (top) the cool-skin temperature correction and (bottom) the net interfacial heat flux.

2.5. COARE Data

Using expressions (12), (13), (14), and (17), we have computed estimates of the cool skin for the *Moana Wave* COARE data. Details of the measurements are given elsewhere [*Fairall et al.*, 1996b; E. F. Bradley et al., Ship-based air-sea flux measurements during TOGA COARE, submitted to *Journal of Atmospheric and Oceanic Technology*, 1995]. These measurements are summarized here as follows: turbulent fluxes are estimated in three different ways (including ship motion-corrected covariances); radiative fluxes are measured with conventional pyranometers and pyrgeometers; and the bulk near-surface water temperature was measured with a thermistor that floated in the upper few centimeters of the ocean. The average model-derived diurnal cycles of ΔT_c and $Q - \delta S_c$ are shown in Figure 1 for the entire data set (1622 50-min samples) and for the cases where the 10-m wind speed is less than 4.0 m s^{-1}. The average nighttime value is about 0.3 K, and the average daytime value is about 0.2 K. In Figure 2 we show the same quantities averaged as a function of wind speed broken down into day and night cases. Note that the ocean convective effect causes the nighttime cool skin to reach a maximum value of about 0.35 K at 1.5 m s^{-1}. In Figure 3 we compare our parameterization with results from the two recent measurement studies described earlier. *Schluessel et al.* [1990, equation (11)] gave a simple linear regression of the cool skin for the nighttime case in terms of the bulk parameters that is indicated by the circles in Figure 30. *Coppin et al.* [1991] stated that for wind speed greater than 1.5 m s^{-1} the simple *Saunders* [1967] formula with $\lambda = 6.5$ fits the average of their measurements (shown in Figure 3 by the crosses). Notice the substantial disagreement of these two parameterizations at low wind speeds. This points out the

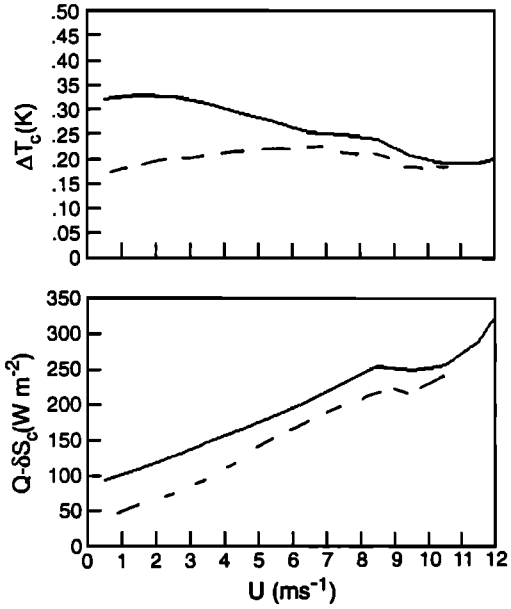

Figure 2. Average cool-skin correction behavior from *Moana Wave* COARE data computed with the cool-skin model versus the mean 10-m wind speed for daytime (dashed lines) and nighttime (solid lines); (top) the cool-skin temperature correction and (bottom) the net interfacial heat flux.

necessity of using a more general, physically based model (see also *Wick et al.* [1996]).

The R/V *Franklin* and the R/V *Vickers* made direct measurements of the sea surface interfacial temperature using special IR radiometers [*Coppin et al.*, 1991; *Wick et al.*, 1996]. We can estimate the total cool-skin temperature difference at night by comparing the radiometer with a bulk temperature from the ship's thermosalinograph. At night, convective mixing tends to destroy the warm layer, so the only process leading to a difference in the skin temperature and the bulk temperature is the cool skin. This is only true after sufficient time has passed to mix out the residual warm layer from the afternoon warming cycle. Comparisons of the computed and measured nighttime cool skin from the *Vickers* are shown in Figure 4. Despite the small range of values, the correlation is fairly good, but the model underestimates the measured difference by 0.05 K. The comparison with the *Franklin* measurements is less favorable (see section 4.1).

3. The Warm Layer

3.1. Warm-Layer Backgrounds

On a clear day the Sun deposits an average of about 500 W m^{-2} of heat into the ocean over the 12 daylight hours. Roughly half of this heat is absorbed in the upper 2 m. The details are dependent on water clarity. In the absence of mixing this is sufficient heat input to warm this 2-m-deep layer uniformly by 2.0 K. Observations [*Price et al.*, 1986; *Fedorov and Ginsburg*, 1992] show that the region of significant warming begins near the surface and propagates downward as it intensifies with increasing solar intensity. Under light wind conditions the near-surface warming can be quite abrupt in the morning and even peak before local noon. Measurable warming occurs as deep as 20 m and may persist well past sundown. Because the majority of the solar heat is deposited in the upper 2 m and the warming leads to a stably stratified surface layer, the turbulence necessary to mix this heat deeper into the mixed layer can only come from shear driven by wind. Thus the characteristic depth of the warm layer D_T is smaller in light winds, and the temperature increase across the warm layer is greater. We also define (analogously to δS_c) the mean solar heat flux instantaneously absorbed in the warm layer as δS_w. In the introduction we discussed the difference between our subsurface in situ temperature measurements (at depth z_r) and the true

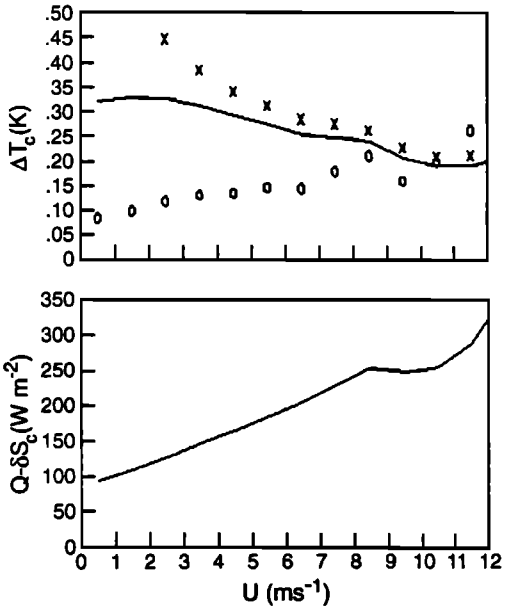

Figure 3. Same as Figure 2, except the crosses are the *Saunders* [1967] model with $\lambda = 6.5$, as described by *Coppin et al.* [1991], and the circles are from *Schluessel et al.* [1990, equation (11)].

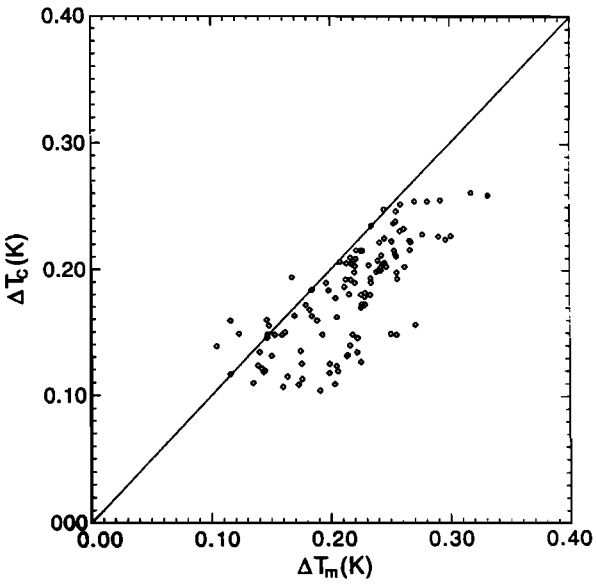

Figure 4. Difference between measured sea surface interface temperature and thermosalinograph bulk temperature versus calculations of the cool-skin temperature difference via (12), (13), (14), and (17).

interfacial surface temperature in the context of (1). Recall that the warm-layer correction depends on the depth of our sensor; the shallower the sensor, the smaller the correction. Because the warm layer may be only a few meters deep on some days, we anticipate that an in situ sensor at one tenth this depth (say, 10 cm) may require warm-layer corrections of the order of tenths of degrees; a sensor at 1 m may require corrections of the order of degrees. This simple scaling analysis suggests that a sensor at 1 cm depth will not require a significant correction for the warm layer, but we examine this point more critically in section 3.2.

The physics of the cool skin are dominated by molecular transport processes with very rapid timescales and small spatial scales that are amenable to laboratory investigation. The same is usually not true for the warm layer. The vertical distribution of the warm layer is determined by a combination of the radiation absorption profile plus molecular and turbulent mixing processes on vertical scales of centimeters to tens of meters. The absorption profile is straightforwardly handled by expressions such as (16), although more attention must be paid to the clarity of the water. This is typically done by using the Jerlov classifications [*Fedorov and Ginsburg*, 1992].

3.2. The Case of Pure Molecular Conduction

While we believe that turbulent mixing is usually important in describing the warm layer, it is instructive to ponder some analytical solutions for purely molecular heat conduction (taken from *Carslaw and Jaeger* [1971]). For a semi-infinite medium initially at temperature T_b with a constant surface flux F_0 (equal to $F_i R_{ns}$ for each appropriate component in Table 1), the temporally asymptotic (after initial transient behavior) difference in the surface temperature and the temperature at depth z_r is

$$T_s - T(z_r) = \Delta T_w(z_r) = \frac{F_0 z_r}{\rho c_p \kappa} \tag{18}$$

where κ is the thermal diffusivity.

These results are quite informative because they put an upper limit on the temperature errors we can expect in the absence of wind mixing. For example, for a sensor at 1 cm depth the last four components in Table 1 are effectively surface sources and the fifth contributes modestly to ΔT_w. Therefore we expect that

$$\Delta T_w(z_r = 0.01) = \frac{[(0.13 + 0.06)\, R_{ns} - Q]}{\rho c_p \kappa}\,(0.01) \tag{19}$$

describes the temperature error of a sensor at 1 cm depth. A net solar flux of 950 W m^{-2} and Q of 100 W m^{-2} gives a temperature error of 2.5 K. Of course, these large surface warmings cannot actually occur because increases in T_s will cause increases in Q, which will quickly limit the warming process. However, this clearly implies that we must not be cavalier in assuming that a sensor at 1 cm depth provides an unambiguous measurement of the surface temperature in very light winds.

3.3. The Price-Weller-Pinkel Turbulent Mixing Model

Price et al. [1986] described the essential turbulent dynamical processes in the development of the PWP mixed-layer model. For our warm-layer model we use a much simplified form of PWP that ignores full mixed-layer dynamics (e.g., seasonal thermocline entrainment). These can be crudely summarized by assuming that once the stratified warm layer forms shortly after δS_w exceeds Q, then the temporal integrals of the surface fluxes induce changes in the near-surface temperature and current that are confined to a depth of D_T:

$$\Delta T_w = \frac{2\int(\delta S_w - Q)\,dt}{\rho c_p D_T} = \frac{2I_S}{\rho c_p D_T}$$
$$\Delta u_w = \frac{2\int u_{*w}^2\,dt}{D_T} = \frac{2I_\tau}{D_T} \tag{20}$$

where u denotes the magnitude of the current. Here we draw a distinction between ΔT_w, the total temperature change across the warm layer, and $\Delta T_w(z_r)$, the warm-layer correction for our sensor at depth z. Note that in this context, δS_w is a function of D_T through (16), where D_T is substituted for δ. The factor of 2 in (20) appears because we assume that the profile is linear from the bottom of the layer to the surface. The depth is determined by requiring the bulk Richardson number to be no greater than a critical value, $R_{ic} = 0.65$:

$$D_T = (2R_{ic})^{1/2}\,\frac{I_\tau}{(\alpha g I_S/\rho c_p)^{1/2}} \tag{21}$$

This depth can be combined with (20) to yield an estimate of the temperature gradient:

$$\frac{\Delta T}{\Delta z} = \frac{\alpha g (I_s/\rho c_p)^2}{R_{ic} I_\tau^2} \tag{22}$$

For illustrative purposes, let us assume that the time integrals over some time interval t can be approximated as $<\delta S_w - Q> t$ and $<u_*^2> t$; then we can write the temperature change between the surface and the depth z_r as

$$\Delta T_w(z_r) = \frac{\alpha g\,(<\delta S_w - Q>/\rho_a c_p)^2}{R_{ic} <u_{*a}^4>}\, z_r \tag{23}$$

Furthermore, if we wish to select a threshold value for an acceptable temperature error, say, ΔT_{th}, then we can estimate the minimum wind speed to achieve the necessary wind mixing:

$$U_{th} = \left[\frac{\alpha g z_r}{R_{ic}\Delta T_{th}}\right]^{1/4}\left[\frac{<\delta S_w - Q>}{\rho_a c_p c_d}\right]^{1/2} \tag{24}$$

For example, if we use a net solar heat flux of 950 W m^{-2} and Q = 100, then a threshold of 0.1 K in (24) gives a wind speed threshold of 0.4 m s^{-1} for z_r = 1 cm and 3.1 m s^{-1} for z_r = 1 m. We can also compute the increase in the water temperature in the upper 2 m by combining (20) and (21). Remember that these are based on approximations to the integrals; more explicit calculations are discussed in sections 3.4–3.6.

3.4. Peak Afternoon Warming During COARE

A simple preliminary investigation has been done with the *Moana Wave* COARE data to look at the peak afternoon warm-layer effects. We selected about 40 days that had a complete diurnal cycle, no big rainstorms, and reasonably constant wind speeds (Table 2). There were additional days of strong winds with no warm layer that we did not include. We took the near-surface bulk temperature just before sunrise as the mixed-layer temperature and found the peak $T(z_r)$ in the afternoon; the difference ΔT_m is the measured solar heating peak (neglecting cool-skin differences). We then computed average solar heat flux $<R_{ns}>$, average net interfacial cooling $<Q>$, and the mean wind speed u. We then estimated the mean u_{*a}^2 as 0.0013 u^2, and computed the PWP model estimate of the total peak warming:

$$\Delta T_w = \left[\frac{2\alpha g t}{R_{ic}\rho}\right]^{1/2} \frac{1}{\rho_a c_p^{3/2}} \frac{[f_w <R_{ns}> - <Q>]^{3/2}}{u_{*a}^2} \quad (25)$$

where t = 7 hours, to cover the period from just after sunrise to just past noon. The factor f_w characterizes the average solar radiation absorbed in the PWP trapping layer, expressed as a fraction of net solar radiation incident at the surface. Rather than using (16), we chose a three-band form of the absorption profile from *Soloviev* [1982] that is deemed appropriate for the moderately clean waters of the COARE region [N = 3; F_i = (0.45, 0.27, 0.28); γ_i = (12.8, 0.357, 0.014) m]:

$$f_w = f(D_T) = 1 - \left\{\sum_{i=1}^{N} F_i \gamma_i \left[1 - \exp(-D_T/\gamma_i)\right]\right\} / D_T \quad (26)$$

Table 2. Some Selected Days From the R/V *Moana Wave* Data During COARE Showing the Peak Solar Warming of the Surface Temperature and the Background Meteorological Information Averaged Over 7 Hours After Sunrise

Q, W m^{-2}	U, m s^{-1}	u_{*a}^2, m^2 s^{-2}	ΔT_m, K	R_{ns}, W m^{-2}	f_w	$\delta S_w - Q$, W m^{-2}	ΔT_w, K	$\Delta T_w(z_r)$, K	D_T, m
280	6.0	0.05	0.2	610	0.77	200	0.1	0	23.0
120	1.3	0.003	1.9	690	0.50	225	2.1	0.1	1.3
160	4.0	0.02	0.3	625	0.66	250	0.4	0	8.0
160	4.0	0.02	0.4	780	0.64	340	0.6	0	7.0
150	3.0	0.011	0.8	640	0.60	235	0.8	0	5.0
140	2.5	0.008	1.2	700	0.57	260	1.0	0	3.3
115	2.0	0.005	0.9	560	0.55	190	1.0	0	2.5
165	3.2	0.013	0.5	650	0.62	240	0.6	0	5.5
145	3.4	0.015	0.9	670	0.62	275	0.6	0	6.0
135	3.5	0.016	0.7	700	0.63	300	0.6	0	6.0
155	5.0	0.032	0	415	0.75	160	0.11	0	16.0
205	5.8	0.043	0.2	450	0.79	150	0.08	0	23.0
260	6.0	0.057	0	230	0.81	0	0	0	100.0
180	4.6	0.021	0.5	680	0.66	230	0.4	0	9.0
200	5.3	0.036	0	350	0.81	80	0.04	0	26.0
130	1.6	0.004	2.0	730	0.52	250	1.9	0.1	1.7
135	1.8	0.004	1.5	590	0.53	180	1.2	0	1.9
150	2.9	0.01	0.6	660	0.59	240	0.7	0	4.3
185	3.6	0.017	0.6	690	0.64	260	0.5	0	7.0
115	1.2	0.002	2.2	710	0.46	215	3.0	0.1	0.9
140	2.2	0.006	0.7	680	0.55	240	1.1	0	2.5
175	5.6	0.042	0.1	360	0.80	115	0.06	0	26.0
190	5.0	0.032	0.2	480	0.75	165	0.1	0	17.0
165	4.1	0.022	0.2	430	0.70	140	0.15	0	12.0
260	9.4	0.11	0	560	0.88	230	0.06	0	48.0
200	9.7	0.12	0	640	0.87	360	0.1	0	42.0
190	5.6	0.042	0.2	680	0.74	310	0.25	0	16.0
160	3.5	0.016	0	245	0.77	30	0.02	0	20.0
100	1.9	0.005	0.3	350	0.57	100	0.4	0	3.3
130	2.9	0.11	0.2	310	0.66	75	0.1	0	8.0
110	1.3	0.002	2.5	610	0.47	180	2.3	0.1	1.0
120	3.0	0.012	0.9	610	0.61	250	0.6	0	5.0
130	3.6	0.018	0.6	615	0.64	270	0.5	0	7.5
130	2.2	0.007	1.1	730	0.56	280	1.3	0	2.7
160	5.0	0.032	0	275	0.88	0	0	0	100.0
175	4.0	0.02	0.6	560	0.67	200	0.3	0	9.0
200	5.0	0.032	0.5	730	0.70	310	0.3	0	12.0
130	3.4	0.015	0.7	700	0.62	300	0.7	0	5.6
145	3.2	0.013	0.5	590	0.62	220	0.5	0	5.6
175	4.2	0.022	0.5	750	0.66	320	0.5	0	8.0
105	3.0	0.012	0.3	350	0.64	120	0.2	0	7.5
130	2.9	0.011	0.4	500	0.66	180	0.4	0	5.5

Variables are defined as follows: Q, total cooling at the interface; U, wind speed; u_{*a}^2, friction velocity for air; ΔT_m, measured solar heating peak; R_{ns}, solar heat flux; f_w, average fraction of solar radiation absorbed in the trapping layer; $\delta S_w - Q$, net heat flux absorbed in the warm layer; ΔT_w, model-computed solar heating peak using (25); $\Delta T_w(z_r)$, temperature change between the surface and the sensor at 5 cm depth; D_T, depth of warm layer.

Note that (21) and (26) must be solved iteratively before we can calculate (25). The comparison between this equation and the values of ΔT_m (computed as described above) for the *Moana Wave* COARE data is shown in Figure 5. In Figure 6 we show a comparison of ΔT_m normalized by $(\delta S_w - Q)^{3/2}$ versus $1/u_{*a}^2$, which from (25) we expect to be linear. Note that the slope through this data is about 1.7×10^{-6}, as implied by (25), with $R_{ic} = 0.65$ as per PWP. For light winds, when the warm layer is most important, this result is fairly insensitive to the choice of R_{ic}. Using (25) and (26), we have constructed typical total warm-layer afternoon peaks as a function of wind speed for essentially cloud-free skies (see Table 3). At a wind speed of 5 m s^{-1} the correction for a sensor at 1-m depth is less than 0.1 K (i.e., $1/10 \times 0.4$), but at 1 m s^{-1} the correction is the full 3.8 K (because $z_r > D_T$).

On the assumption that the *Moana Wave* water temperature sensor may not be measuring the true surface temperature during very light winds, we computed the correction for a sensor at depth z_r using (23). Using a value for z_r of 5 cm, which is an upper limit for a realistic number, there is little difference (see the column labeled $\Delta T_w(z_r)$ in Table 2).

3.5. Morning Onset of the Warm Layer

The PWP model describes the dynamical processes in the development of the near-surface turbulent layer. To describe the initial onset of the warm layer, it is useful to introduce the concept of the "compensation depth" D_c [*Woods and Barkmann*, 1986]. D_c is the depth at which the absorbed solar radiation exactly compensates the surface heat loss Q; D_c is defined by

$$f(D_c)\, R_{ns}(t) = Q \tag{27}$$

where we explicitly note the strong time dependence of R_{ns}. PWP assume that all relevant quantities, heat, salt, and momentum, are mixed instantaneously to depth D_c by convectively driven overturns. For typical transparency profiles, D_c shallows very rapidly as $R_{ns}(t)$ increases during the first few hours of a clear morning; beneath D_c, turbulence ceases unless mechanical energy is provided to support it. PWP's essential assumption is that, at certain times in the morning, the velocity induced by the shear stress above the rapidly shallowing D_c starts to increase so rapidly that it induces Kelvin-Helmholtz instability in the heated water above D_c. After that time the mixing depth is controlled by a Richardson number criterion rather than by the compensation depth (as described above). However, considerations of D_c permit a more rigorous determination of the time when the warm-layer discontinuity occurs.

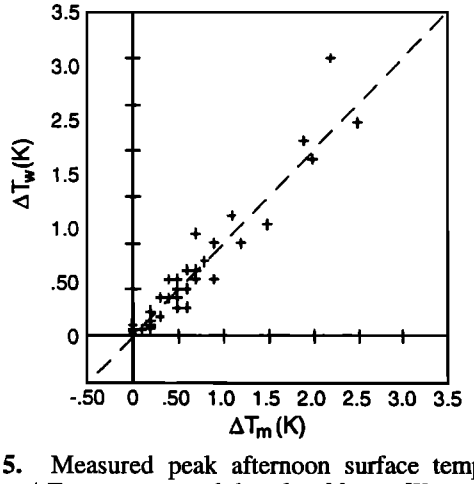

Figure 5. Measured peak afternoon surface temperature warming ΔT_m as measured by the *Moana Wave* floating sensor, referenced to its presunrise value, which is assumed to represent the "bulk" mixed-layer temperature; ΔT_w is computed using (25).

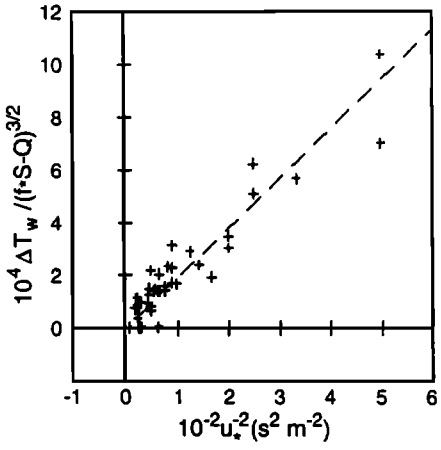

Figure 6. Measured peak afternoon surface temperature warming normalized by the 3/2 power of $\delta S_w - Q$ versus u_{*a}^{-2}.

From (20) we note the accumulation of momentum and heat in the near-surface zone. For short timescales the surface stress can be considered constant around onset, so it can be extracted from the time integral. The net heat transfer within the layer is zero at onset, so we can expand it to first order in time and then perform the integrals defined in (20). The result is

$$\begin{aligned} I_\tau &= u_{*w}^2 (t - t_0) \\ I_S &= \frac{f(D_T)}{2\rho c_p} \frac{\partial R_{ns}}{\partial t} (t - t_0)^2 \end{aligned} \tag{28}$$

where t_0 is the time of onset and we assume that at onset $D_c = D_T$. Using (21), we can solve for D_T at onset with f_0 the value of $f(D_T)$:

$$f_0 D_T^2 = \frac{4\rho c_p u_{*w}^4 R_{ic}}{\alpha g \dfrac{\partial R_{ns}}{\partial t}} \tag{29}$$

For a clear morning we can approximate the time dependence of the solar flux with a simple sine function, $R_{ns} = S_0 \sin(\omega t)$, so that (using (27) to determine the time of onset)

$$f_0 D_T^2 \approx \frac{4\rho c_p u_{*w}^4 R_{ic}}{\alpha g \omega S_0 \left\{1 - \left[Q/(f_0 S_0)\right]^2\right\}^{1/2}} \tag{30}$$

Table 3. Warm-Layer Afternoon Peak As a Function of Wind Speed for Nearly Cloud-Free Conditions During COARE

U, m s^{-1}	R_{ns}, W m^{-2}	Q, W m^{-2}	f_w	$f_w \times R_{ns} - Q$	u_{*a}^2, m^2 s^{-2}	D_T, m	ΔT_w, K
1	710	100	0.44	210	0.0015	0.7	3.8
2	710	110	0.54	270	0.0052	2.1	1.6
3	710	125	0.59	300	0.011	4.2	0.9
4	710	165	0.63	280	0.016	6.0	0.6
5	710	190	0.68	290	0.025	10.0	0.4
6	710	230	0.72	280	0.034	14.0	0.25
7	710	260	0.76	280	0.049	19.0	0.15

See Table 2 for definitions.

where S_0 is the noon net solar flux, t is the time after sunrise, and ω is the diurnal angular frequency. The time of warm-layer onset is simply given by

$$t_0 = \frac{1}{\omega} \sin^{-1}\left[Q/(f_0 S_0)\right] \tag{31}$$

Using (26), we can solve (30) for typical COARE parameters; the results for different wind speeds and essentially clear days are shown in Table 4. These calculations suggest that the warm-layer onset occurs about an hour after sunrise. However, from (20) and (28), ΔT_w rises quadratically after onset, so it may be another hour or so before the effect is noticeable. When applying the warm-layer model to a time series of data, the results shown in Table 4 can be used as a first guess for f and D_T and the time of onset, or (29) can be solved with explicit calculations of $\partial R_{ns}/\partial t$. Rapid increase in T_s occurs shortly after onset. Figure 7 shows an example of data from multiple near-surface temperature sensors compared with a detailed, multilayer PWP model calculation [*Ravier-Hay and Godfrey*, 1993]. The formation of a thin layer near 0930 local standard time (LST) is very apparent on this day for which the skies were clear and wind speeds were below 1 m s^{-1} until shortly after noon, when winds increased rapidly in association with a rain storm. This strongly suggests that the basic assumptions of the PWP scaling model and the implication for the onset of the warm layer are reasonable.

3.6. The Average Heating Cycle During COARE

The analysis presented so far is for the onset and peak warming of the warm layer. On the grounds that it would be interesting to see if this simple model reproduces the hourly evolution of the diurnal cycle with any accuracy, we again processed the *Moana Wave* 50-min data. Starting at midnight (LST) of each measurement day, we initialized D_T at 19 m and set I_S and I_τ to zero. Beginning at the time when $f_w R_{ns} - Q$ first exceeds zero, we computed the time integrals as described by (20). Measured values of ΔT_w were defined as the difference in in situ measured near-surface temperature at the subsequent times and the near-surface temperature at this initial time. Note that (21) and (26) were solved iteratively to give self-consistent values for D_T and f_w. The average diurnal cycle of measured and computed ΔT_w and computed D_T is shown in Figure 8a for the 51 measurement days, where the average daytime value of u_{*a}^2 was less than 0.05 m^2 s^{-2} (i.e., wind speed less than about 6.5 m s^{-1}). To illustrate the effects of wind speed, we show the same diurnal averages for $0.02 < u_{*a}^2 < 0.05$ (Figure 8b) and $u_{*a}^2 < 0.008$ (Figure 8c). Notice the asymmetry of the signatures for the lighter wind case. The warm layer becomes quite shallow (1 m) almost immediately and deepens steadily through the day; the surface temperature rises very quickly and peaks just after noon, with some residual warming still present at midnight.

Table 4. Warm-Layer Onset As a Function of Wind Speed for Nearly Cloud-Free COARE Conditions

U, m s^{-1}	t_0, h	Q, W m^{-2}	f_0	$R_{ns}(t_0)$, W m^{-2}	D_T, m
1	0.91	100	0.45	223	0.77
2	0.83	110	0.54	203	2.2
3	0.86	125	0.59	211	4.3
4	1.08	165	0.62	265	6.0
5	1.18	190	0.66	287	9.0
6	1.37	230	0.69	331	12.0
7	1.47	260	0.73	354	16.0

See Table 2 for definitions; t is time.

4. Combining the Cool-Skin and Warm-Layer Corrections

4.1. Simulating the Diurnal Cycle

The cool-skin and warm-layer corrections described in the previous sections have been combined and integrated into the standard bulk flux algorithm [*Fairall et al.*, 1996a] for the COARE program (presently designated as COARE version 2.0). The algorithm requires inputs of bulk water temperature, wind speed, and air temperature and humidity as is normal for bulk computations, plus inputs of downward solar and longwave irradiance that are required for the warm and cool correction components. Additional required input parameters are the height of the atmospheric sensors, the depth of the water temperature sensor, and associated information such as surface atmospheric pressure and local (solar) time of each observation. The transfer coefficients have been tuned to yield correct fluxes when cool-skin and warm-layer effects are incorporated in the computations. By starting at the beginning of a data sequence, the algorithm can be used to estimate the surface temperature corrections and compute the fluxes in a consistent manner. Note that if this model is applied as an upper boundary condition for an oceanic mixed-layer model, then the warm-layer part is not

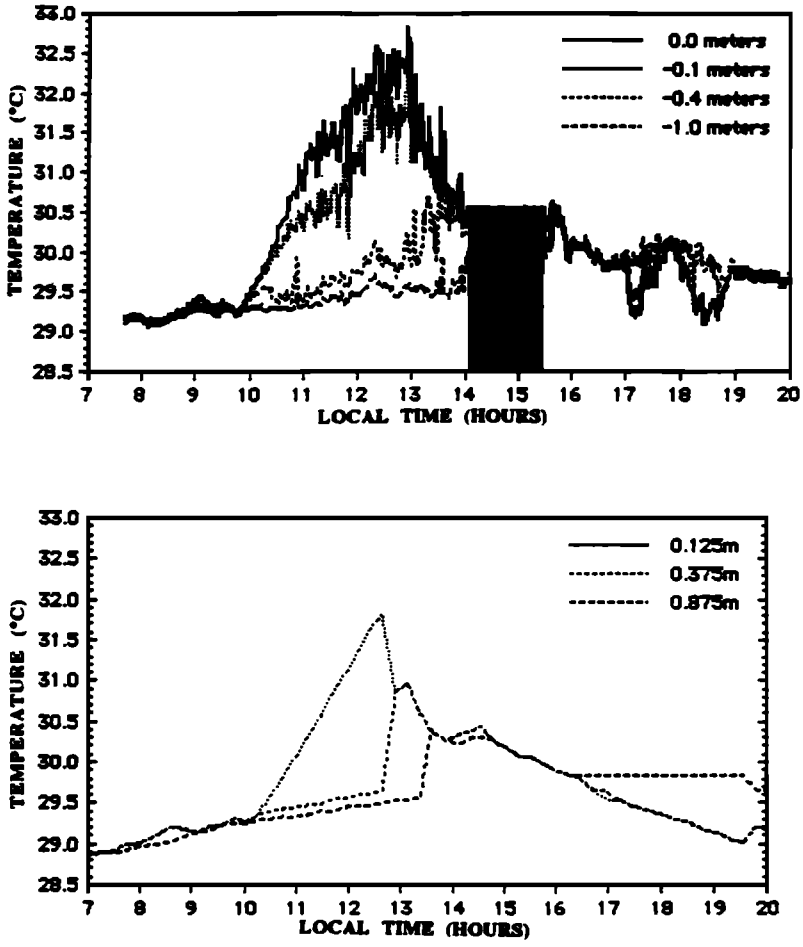

Figure 7. Near-surface oceanic temperatures from *Ravier-Hay and Godfrey* [1993]: (top) measurements and (bottom) Price-Weller-Pinkel (PWP) [*Price et al.*, 1986] model computations at 0.125-m resolution. The solid rectangle (top) indicates a period of wind and rain associated with a storm.

required if the oceanic model has sufficient vertical (and temporal) resolution to accurately resolve the diurnal warm layer.

An example of the resultant total cool-skin and warm-layer magnitudes is given in Figure 9 for a 4-day sequence from the *Moana Wave* data. Notice that on the first 2 days the winds are fairly strong and the total warm layer is quite small. Also, the diurnal variation of the cool skin is substantial, with almost no cool-skin correction at all during much of the sunlight period on day 318.

We have also used measurements from the R/V *Franklin* to examine the accuracy of the model corrections. A sample 5-day period from early December 1992 is shown in Figure 10. In this figure the thermosalinograph temperature measured at a depth of 2.0 m is clearly missing the large diurnal cycle of SST indicated by the IR thermometer. We have taken the cool-skin and warm-layer corrections from the model to estimate the true interfacial temperature from the thermosalinograph; this is the third curve shown in Figure 10. The amplitude of the model-computed warming on the first 3 days is slightly smaller than measured, and the phase lags the observations by about 1 hour. The model appears to provide corrections for these 3–4 K errors with an accuracy of about ±0.5 K. Notice also that on two of the five nights the model accurately captures the cool skin, but on the other three nights the measurements indicate that essentially no cool skin exists (i.e., the IR and thermosalinograph temperatures are very close). This does not seem physically plausible, so we suspect that some residual warm-layer effects remain that are not predicted by the model or that the measurements are in error. The nighttime IR SST data were unusually noisy during COARE, so problems with this sensor cannot be ruled out at this stage.

4.2. Effects on the Average COARE Energy Budget

Using the *Moana Wave* data, we have computed mean bulk-derived values for sensible and latent heat fluxes. When combined with net solar and IR radiative fluxes, these yield a value to the total heat supplied by the atmosphere to the surface of the ocean:

$$H_{tot} = R_{ns} + R_{nl} - H_s - H_l \tag{32}$$

The results of the average computations are given in Table 5. These averages represent 1622 50-min samples taken over 70 days in the following periods: November 11–December 3, 1992; December 17, 1992–January 11, 1993; and January 27–February 16, 1993. Also shown in Table 5 are the fluxes that result when the cool-skin correction is

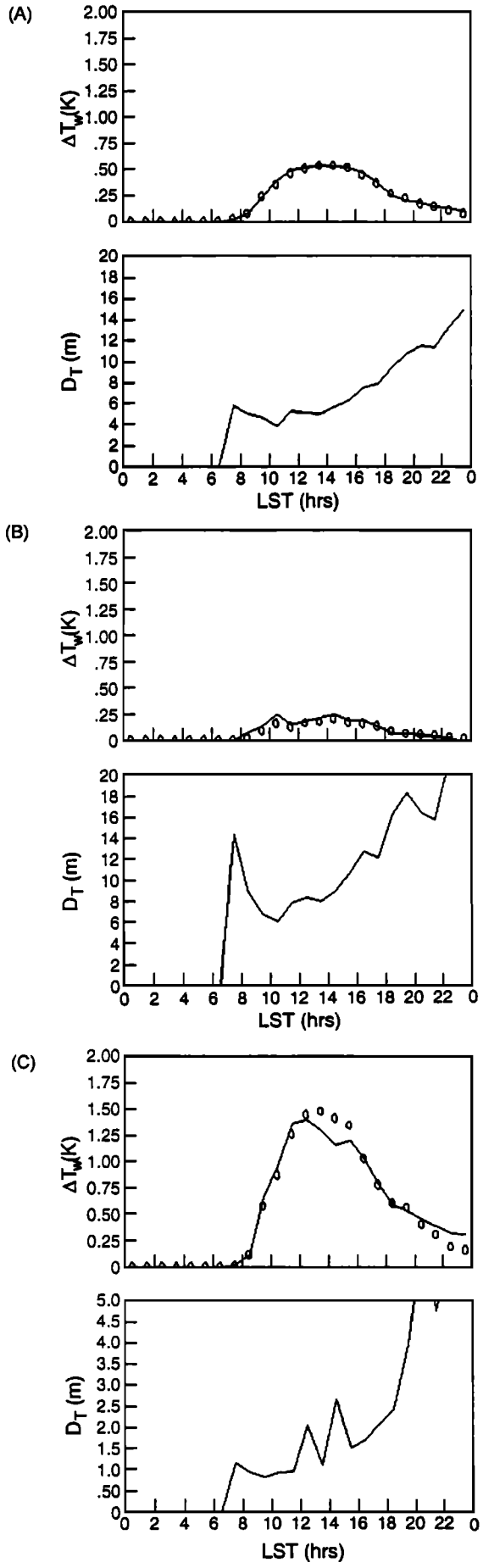

turned off or when a 2-m water temperature is used without a warm-layer correction. Excluding the cool skin increases the net warming of the ocean by 11 W m^{-2}, while using an uncorrected 2-m water temperature for the SST reduces the net warming by 4 W m^{-2}. *Cornillon and Stramma* [1985] estimated a 5 W m^{-2} reduction in heat flux from diurnal warming observed with satellite measurements of SST in the North Atlantic. The effect is primarily realized in the latent heat flux, which is about 3 times the effect in either the sensible heat flux or the net longwave cooling. For the COARE data the average net effect of neglecting both corrections is only about 5 W m^{-2}. However, it is important to note that these processes tend to operate at different parts of the diurnal cycle. Thus they significantly intensify the diurnal cycle of the surface forcing of the atmospheric boundary layer. In regions with stronger winds the warm-layer effect will be negligible, but the cool-skin effect on the energy budget will actually be increased. The small size of the average warm-layer effect is because the very large temperature errors occur in very light winds when the fluxes tend to be small. For example, for a wind speed of about 1 m s^{-1} a peak warming of 2 K will occur that will affect the total surface energy budget by roughly 50 W m^{-2}, but only for a few hours out of the day.

5. Conclusions

SST (i.e., the actual ocean-air interfacial temperature) is a key variable driving air-sea interaction. Uncertainties in the air-sea temperature difference represent a major uncertainty in assessing the heat balance of the tropical western Pacific warm pool; to estimate this heat balance to an accuracy of 10 W m^{-2} requires specification of the SST to an accuracy of ±0.2 K. Even precisely calibrated bulk-water temperature sensors are often not able to achieve this accuracy because of two types of sampling error: the warm layer and the cool skin. Thus to obtain bulk flux estimates approaching the accuracies desired for COARE, bulk-water temperature data from ships and buoys must be corrected for these effects.

In this paper we have described some of the physics associated with both the cool-skin and warm-layer effects and developed models to estimate corrections for water temperature sensors. These models have been integrated into a bulk flux routine. This has the advantage that the flux variables required by the models and the temperature corrections needed in the bulk flux routine can be solved iteratively in a self-consistent manner. The cool-skin model is based on the standard *Saunders* [1967] treatment modified to include both shear-driven and convectively driven turbulence through their relative contributions to the near-surface turbulent kinetic energy dissipation rate. The dissipation rate directly affects the thickness of the cool-skin

Figure 8. Average diurnal behavior from *Moana Wave* COARE data computed with the PWP warm-layer scaling model. (top) The warm-layer surface temperature difference, measured (solid lines) and model computed (circles). (bottom) The computed warm-layer depth. (a) All days with daytime mean $u_{*a}^2 < 0.05$ m^2 s^{-2} (n = 51). (b) All days with daytime mean $0.02 < u_{*a}^2 < 0.05$ m^2 s^{-2} (n = 20). (c) All days with daytime mean $u_{*a}^2 < 0.008$ m^2 s^{-2} (n = 10).

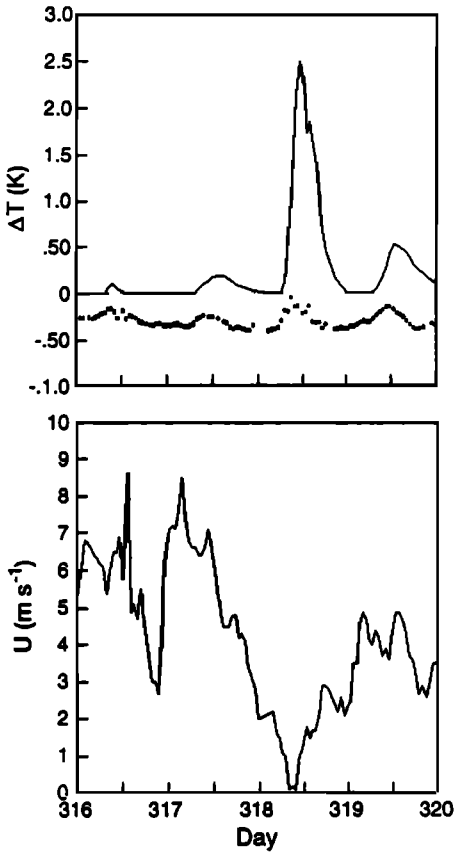

Figure 9. Sample diurnal variations from 4 days of measurements of the *Moana Wave* during the COARE experiment. (top) The warm-layer (solid line) and cool-skin (dots) corrections computed from the model. (bottom) The wind speed.

Table 5. Average Bulk Surface Energy Budget Terms From the *Moana Wave* Data From COARE

Model	H_s	H_l	R_{ns}	R_{nl}	H_{tot}
Cool and warm	7.7	103.3	191.5	-57.1	23.4
No cool	9.6	110.8	191.5	-58.7	12.4
No warm	7.3	100.7	191.5	-56.1	27.4

All values are in watts per square meter. H_s and H_l are sensible and latent heat fluxes, respectively. R_{ns} and R_{nl} are net shortwave and longwave radiation, respectively.

layer; this effect is incorporated into the model through a buoyancy-dependent "Saunders coefficient." For shear-driven conditions the Saunders coefficient is given a value of 6; it decreases as wind speed decreases. Shear and convective effects are comparable at a wind speed of about 2.5 m s^{-1}, yielding a Saunders coefficient of 4.8. A simplified form of *Paulson and Simpson*'s [1981] solar absorption parameterization is used to account for the reduction in the cool skin by solar heating in the upper millimeter of the ocean. For the R/V *Moana Wave* COARE data the model gives an average cool skin of 0.30 K at night and an average local noon value of 0.18 K. The model gives somewhat larger cool skins than were observed with an IR radiometer aboard R/V *Franklin* during COARE, but it yields somewhat smaller cool skins than were observed aboard R/V *Vickers*.

The warm-layer model is based on a single-layer scaling version of a model by *Price et al.* [1986]. The model is based on the idea that once solar heating of the ocean exceeds the combined cooling by turbulent scalar heat transfer and net longwave radiation, then the main body of the mixed layer is cut off from its source of turbulence. Thereafter, surface inputs of heat and momentum are confined to a depth D_T, which is determined by the subsequent integrals of the heat and momentum subject to a

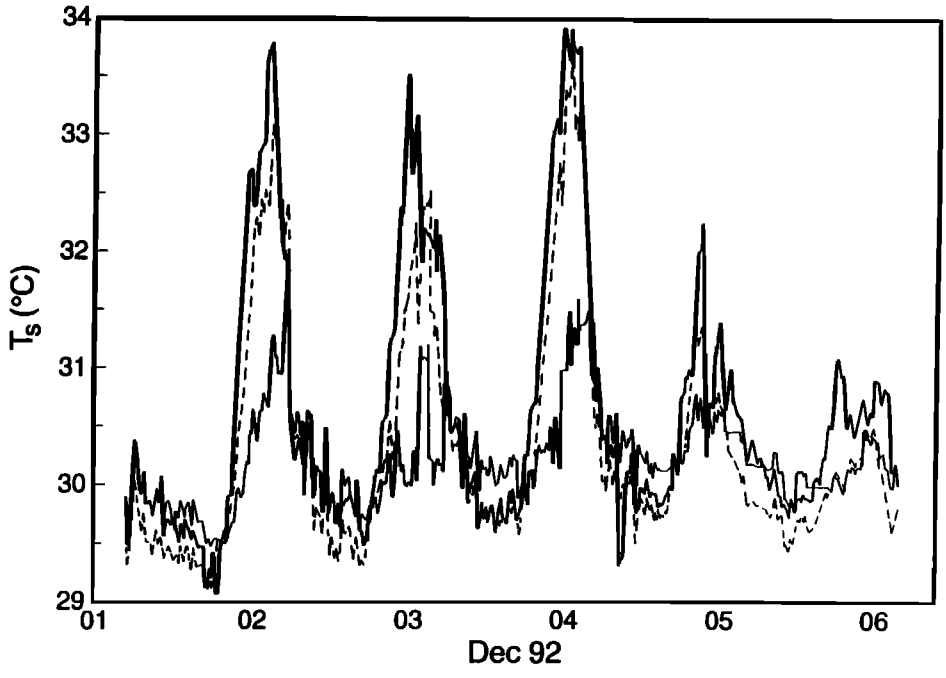

Figure 10. Sample diurnal surface temperature measurements from the R/V *Franklin* during COARE. The thin solid line is the thermosalinograph at a depth of 2 m; the thick solid line is the IR thermometer; and the dashed line is the model correction added to the thermosalinograph.

Richardson number criterion. The model assumes linear profiles of temperature and surface-stress-induced current in this "warm layer." The so-called compensation depth (i.e., the depth at which the total absorbed solar radiation first exceeds surface cooling) is shown to be useful in describing the onset of this surface decoupling, which typically occurs about 1 hour after sunrise on a clear day. Averaged over 40 days from the COARE experiment, the model is shown to describe the peak afternoon warming and the diurnal cycle of the warming quite accurately with the choice of a critical Richardson number of 0.65 (the value used by PWP). For a clear day with a 10-m wind speed of 1 m s^{-1}, the peak afternoon warming is about 3.8 K, decreasing to about 0.2 K at a wind speed of 7 m s^{-1}. In light wind conditions, D_T tends to be shallowest at onset and to deepen slightly during the day; after sunset it deepens more rapidly, but even at midnight some measurable warming still persists.

The integrated bulk flux routine with both cool skin and warm layers was tested against selected COARE data. Besides the standard bulk meteorological variables, this integrated model requires inputs for downward longwave and shortwave radiative fluxes. These must be provided by direct measurement or estimated in some other way. A sunny, light-wind, 5-day period from R/V *Franklin* was used to examine model predictions of SST; the *Franklin* data included both IR interfacial temperature and thermosalinograph temperature at a depth of 2.0 m. The model underestimated the 3-4 K amplitude of the warming by about 0.5 K and lagged in phase by about 1 hour. For COARE the cool skin increases the average atmospheric heat input the ocean by about 11 W m^{-2}; the warm layer decreases it by about 4 W m^{-2}. The primary effect is through the latent heat flux.

Both the cool-skin and warm-layer models described here show fairly good performance in the COARE region. While physically based parameterizations have been emphasized, the general applicability in other climate regimes is still open to question. The cool-skin approach used here is fairly simple; more complex treatments are given by *Soloviev and Schluessel* [1994] and *Wick et al.* [1996]. We must also point out that the warm-layer model presented here is not rigorous because the simple heat and momentum integrals are not handled in a conservative fashion. For example, if the value of D_T increases with time, solar heat absorbed below D_T prior to the increase is ignored. This may explain the magnitude and phase errors of the model in very light winds. Conversely, if D_T were to decrease (a fairly rare occurrence), all of the heat and momentum previously deposited in the turbulent layer would be squeezed into the new, shallower layer. These issues will be examined in more detail when more of the near-surface ocean temperature and turbulence data from COARE become available.

Acknowledgments. This work was supported by the joint NSF/NOAA Climate and Global Change Program, the Office of Naval Research, the Department of Defense ASAP program, and the CSIRO Climate Change Research Program. Thanks are extended to Bill Emery for a very careful review of this manuscript.

References

Carslaw, H. A., and J. C. Jaeger, *Conduction of Heat in Solids*, 510 pp., Oxford Univ. Press, New York, 1971.

Coppin, P. A., Measurements of sea surface temperature aboard R/V *Franklin* during TOGA COARE, paper presented at the TOGA COARE Data Workshop, Cent. Natl. d'Etudes Spatiale, Toulouse, France, 1994.

Coppin, P. A., E. F. Bradley, I. J. Barton, and J. S. Godfrey, Simultaneous observations of sea surface temperature in the western equatorial Pacific Ocean by bulk, radiative, and satellite methods, *J. Geophys. Res., 96*, 3401–3409, 1991.

Cornillon, P., and L. Stramma, The distribution of diurnal warming events in the western Sargasso Sea, *J. Geophys. Res., 90*, 1811–1815, 1985.

Fairall, C. W., E. F. Bradley, D. P. Rogers, J. B. Edson, and G. S. Young, Bulk parameterization of air-sea fluxes for the Tropical Ocean-Global Atmosphere Coupled Ocean-Atmosphere Response Experiment, *J. Geophys. Res.*, in press, 1996a.

Fairall, C. W., A. B. White, J. B. Edson, and J. E. Hare, Integrated shipboard measurements of the marine boundary layer, *J. Atmos. Oceanic Technol.*, in press, 1996b.

Fedorov, K. N., and A. I. Ginsburg, *The Near-Surface Layer of the Ocean*, pp. 63–108, Koninklije Wohrmann, Utrecht, Netherlands, 1992.

Hasse, L., The sea surface temperature deviation and the heat flow at the sea-air interface, *Boundary Layer Meteorol., 1*, 368–379, 1971.

Lukas, R., Observations of air-sea interaction in the western Pacific warm pool during WEPOCS, paper presented at the Western Pacific International Meeting and Workshop for TOGA COARE, Inst. Fr. de Rech. Sci. pour le Dev. en Coop. (ORSTOM), Noumea, New Caledonia, 1989.

Panofsky, H. A., and J. A. Dutton, *Atmospheric Turbulence*, 397 pp., Wiley-Intersci., New York, 1984.

Paulson, C. A., and J. J. Simpson, The temperature difference across the cool skin of the ocean, *J. Geophys. Res., 86*, 11,044–11,504, 1981.

Price, J. F., R. A. Weller, and R. Pinkel, Diurnal cycling: Observations and models of the upper ocean response to diurnal heating, cooling, and wind mixing, *J. Geophys. Res., 91*, 8411–8427, 1986.

Ravier-Hay, P., and J. S. Godfrey, A model of diurnal changes in sea surface temperature for the western equatorial Pacific, *TOGA Notes, 11*, pp. 5–8, Nova Southeast. Univ., Dania, Fla., 1993.

Robinson, I. S., N. C. Wells, and H. Charnock, The sea surface thermal boundary layer and its relevance to the measurement of the sea surface temperature of airborne and satellite radiometers, *Int. J. Remote Sens., 5*, 19–45, 1984.

Saunders, P. M., The temperature at the ocean-air interface, *J. Atmos. Sci., 24*, 269–273, 1967.

Schluessel, P., W. J. Emery, H. Grassl, and T. Mammen, On the bulk-skin temperature difference and its impact on satellite remote sensing of the sea surface temperature, *J. Geophys. Res., 95*, 13,341–13,356, 1990.

Shigayeva, V. V., S. N. Druzhinin, and V. L. Lebedev, Study of temperature surface film by results of sea observations, *Meteorol. Gidrol., 5*, 75–79, 1982.

Soloviev, A. V., On the vertical structure of the ocean thin surface layer at light wind, *Dokl. Acad. Sci. USSR, Earth Sci. Ser.*, Engl. Transl., *18*, 751–760, 1982.

Soloviev, A. V., and P. Schluessel, Parameterization of the cool skin of the ocean and of the air-ocean gas transfer on the basis of modeling surface renewal, *J. Phys. Oceanogr., 24*, 1339–1346, 1994.

Webster, P. J., and R. Lukas, TOGA COARE: The Coupled Ocean-Atmosphere Response Experiment, *Bull. Am. Meteorol. Soc., 73*, 1377–1416, 1992.

Wick, G. A., W. J. Emery, L. H. Kantha, and P. Schluessel, The behavior of the bulk-skin sea surface temperature difference under varying wind speed and heat flux, *J. Phys. Ocean.*, in press, 1996.

Woods, J. D., and W. Barkmann, The response of the upper ocean to solar heating, I, The mixed layer, *Q. J. Roy. Meteorol. Soc., 112*, 1–27, 1986.

Wyngaard, J. C., and O. R. Cote, The budgets of turbulent kinetic energy and temperature variance in the atmospheric surface layer, *J. Atmos. Sci., 28*, 190–201, 1971.

E. F. Bradley, Centre for Environmental Mechanics, CSIRO, Canberra, A.C.T. 2601 Australia. (email: bradley@python.enmech.csiro.au)

J. B. Edson, Applied Ocean Physics and Engineering Department, Woods Hole Oceanographic Institution, Woods Hole, MA 02543. (email: jedson@airsea2.whoi.edu)

C. W. Fairall, Environmental Technology Laboratory, NOAA, 325 Broadway, Boulder, CO 80303. (email: cfairall@etl.noaa.gov)

J. S. Godfrey, Division of Oceanography, CSIRO, Hobart, Tasmania 7001 Australia. (email: godfrey@ml.csiro.au)

G. A. Wick, University of Colorado, Colorado Center for Astrodynamics Research, Boulder, CO 80309. (email: wickg@frodo.colorado.edu)

G. S. Young, Department of Meteorology, Pennsylvania State University, University Park, PA 16802. (email: gyoung@ems.psu.edu)

(Received April 7, 1995; revised August 28, 1995; accepted September 25, 1995.)